# Revisiting the lattice dynamics of cubic yttria-stabilized zirconia

Shelby R. Turner [1,2,3] Stéphane Pailhès,[3] Leila Ben-Mahfoud,[4] Marc de Boissieu,[2] Frédéric Bourdarot,[5]
Helmut Schober [6] Yvan Sidis [7] John-Paul Castellan,[7,8] Andrea Piovano [1] Alexandre Ivanov [1]
and Valentina M. Giordano [3,*]

[1]*Institut Laue-Langevin, Grenoble, F-38042 Grenoble Cedex, France*
[2]*Université Grenoble Alpes, CNRS, Grenoble-INP, SIMaP, F-38402 St. Martin d'Hères, France*
[3]*Institute of Light and Matter, UMR5306 Université Lyon 1-CNRS, Université de Lyon, F-69622 Villeurbanne Cedex, France*
[4]*Laboratoire Hubert Curien, UMR5516, Université St. Etienne, F-42000 Saint-Etienne, France*
[5]*Université Grenoble Alpes, CEA, IRIG, MEM, MDN, F-38000 Grenoble Cedex, France*
[6]*European Spallation Source ERIC, P.O. Box 176, SE-221 00 Lund, Sweden*
[7]*Laboratoire Léon Brillouin, CEA, CNRS, UMR-12, CE-Saclay, F-91191 Gif-sur-Yvette, France*
[8]*Institut für Festkörperphysik, Karlsruher Institut für Technologie, D-76021 Karlsruhe, Germany*

Cubic yttria-stabilized zirconia has long been a ceramic material of interest for its many uses in thermal-based applications. Its very low and weakly temperature-dependent thermal conductivity has been ascribed to the large oxygen vacancies content, which introduces disorder and strongly scatters phonons. Still, despite many experimental works in the literature, phonon dynamics has not been fully understood yet, with several points to be clarified, such as the apparent absence of optic modes throughout the Brillouin zone. In this paper, we present findings on the phonon dispersions of this material, showing experimental evidence of low-lying optical branches throughout the Brillouin zone, which reduce the pure acoustic regime for some branches. Furthermore, the observed energy dependence of the intrinsic acoustic phonon linewidths clearly suggests the existence of competing Mie and Rayleigh scattering mechanisms. Our findings allow to uncover a different phonon dynamics scenario in this material and point to a deeper understanding of heat transport in yttria-stabilized zirconia, based on two different, concomitant mechanisms, generated by the large vacancy content.

## I. INTRODUCTION

Zirconia ($ZrO_2$) is one of the most studied ceramic materials due to a number of properties which make it suitable for many different applications, such as a high-temperature ion conductor in solid oxide fuel cells, or thermal barrier coating [1–3]. Stable at room temperature in its monoclinic form [4], zirconia transforms to a tetragonal structure at 1440 K [5] and a cubic phase at 2640 K [6]. Its ideal resistance to fracture for a wide temperature range can be further solidified with the addition of rare-earth elements, which impacts the phase diagram, changing the stability regions of the different phases. Specifically, at room temperature, yttria-stabilized zirconia [$(ZrO_2)_{1-x}(Y_2O_3)_x$, YSZ] is monoclinic for $x \lesssim 2$ mol %, tetragonal for $\sim 2 \lesssim x \lesssim 8$ mol %, and cubic for $\sim 8 \lesssim x \lesssim 20$ mol % [7]. This latter phase is characterized by a surprisingly low thermal conductivity, good thermal shock resistance, and a high melting point, a combination of properties that makes it ideal for thermal-barrier applications such as for turbine engines.

The introduction of yttria gives rise to a highly defective crystal with a large amount of oxygen vacancies, proportional to the yttria content [8,9], which causes strong static disorder

and large relaxations, leading to thermal transport properties much different from the ones of a pure zirconia phase. Indeed, while pure, monoclinic zirconia has a room-temperature thermal conductivity of 8.2 W/mK [10] which decreases with temperature, compatible with anharmonic umklapp processes such as the dominant phonon scattering mechanism, the introduction of yttria drastically modifies its value and behavior. First, the thermal conductivity at room temperature decreases with yttria content up to $x = 10$ mol %, where a minimum exists, equal to 2 W/mK. It then increases again with higher concentrations of yttria [10,11], which has been ascribed to a rearrangement of the vacancies into locally ordered aggregates [9–15]. Moreover, at high temperature, independent of the yttria content, the measured value is about 2 W/mK and almost temperature independent [11]. This low value corresponds to the minimum thermal conductivity calculated on the basis of the minimum phonon mean free path, such as in glasses [8]. Such glasslike thermal transport has been ascribed to a dominant defect-induced phonon scattering mechanism above room temperature due to the extended vacancy-defect structure [12–14]. However, a full understanding of the role of oxygen vacancies and their impact on phonon propagation is still missing. From a theoretical point of view, it is extremely difficult to calculate *ab initio* phonon dynamics in YSZ due to the highly defective structure. This is especially true for cubic YSZ with an yttria content in the 9–10 mol % range, in which vacancies are still relatively isolated clusters: This phase is

---

*Author to whom correspondence should be addressed: valentina.giordano@univ-lyon1.fr

characterized by the minimum thermal conductivity and the impact of vacancies can be thus expected to be the strongest. Only a few studies have been reported on the dynamics of this phase, mainly based on molecular dynamics simulations [16,17] with some density functional theory (DFT) calculations [18,19], which mostly concentrate on phonon density of states calculations.

On the experimental side, the lattice dynamics of cubic YSZ have been extensively studied by neutron and x-ray scattering and Raman spectroscopy [19–25]. Inelastic scattering studies revealed the presence of acoustic phonons dispersing up to 20 and 30 meV for transverse and longitudinal polarizations, respectively, exhibiting a strong—although not quantified—broadening, which was ascribed to the important defect scattering and suggested as responsible for the glasslike thermal transport properties [20]. Surprisingly, no optical mode could be observed, despite their report in Raman studies [21,23,24]. As these modes are due to the out-of-phase vibrations of the two oxygen sublattices, it was argued that disorder in these latter would strongly affect the optical modes, such that they would not be well defined except at the $\Gamma$ point [19–21].

In order to definitively understand thermal transport in cubic YSZ, an exhaustive and high-resolution measurement of its phonon dynamics is still needed which specifically addresses the quantitative measurement of the acoustic phonon lifetime, the key parameter for all thermal conductivity calculations and for elucidating the dominant scattering mechanisms. This is the aim of this work. Here, we present a combined inelastic neutron and x-ray scattering (INS, IXS) investigation of the phonon dynamics in a single-crystal YSZ with 9.5 mol % yttria concentration.

Owing to a higher resolution with respect to previous studies, we could uncover a deeper understanding of the lattice dynamics in YSZ. Here, we report experimental evidence in the full Brillouin zone of optical modes in YSZ, which extend up to ∼35 meV. The lowest-lying optical mode, centered at 9 meV, is found to interact with the acoustic modes, marking a premature end of the pure acoustic regime. Our findings allow us to revisit the phonon dynamics in YSZ and suggest another interpretation of the mechanisms leading to its glasslike thermal transport.

## II. RESULTS AND DISCUSSION

INS measurements were made on a 1 cm³ cube sample (CrysTec) at the Laboratoire Léon Brillouin (LLB) and the Institut Laue-Langevin (ILL), using the thermal-neutron triple-axis spectrometers (TAS) 1T@LLB and IN8@ILL and a fixed $k_f = 2.662$ Å$^{-1}$, and 20′ collimation on 1T@LLB. Further measurements were done at the cold-neutron TAS 4F2 at the LLB, using a fixed $k_f = 1.48$ Å$^{-1}$ and the Be filter. IXS measurements were made on a ∼0.001 mm³ sample at the ID28 beamline of the European Synchrotron Radiation Facility (ESRF), using the [999] reflection of the silicon monochromator, which provides an energy resolution of 2.8 meV. The sample was mounted on a needle and the measurements were performed in transmission geometry. More details can be found in the Supplemental Material Appendix B [26] and references therein [27,28].
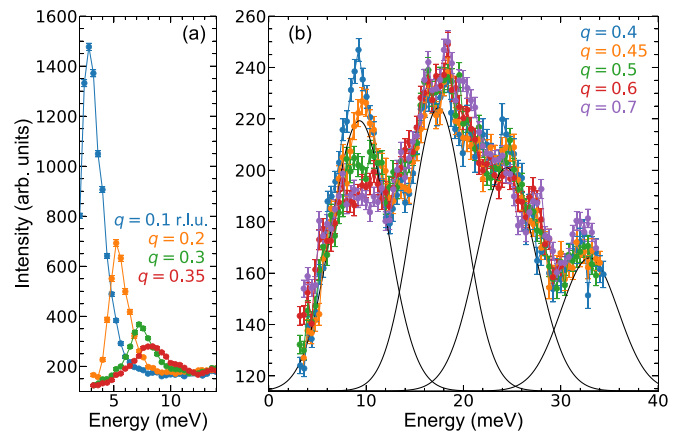


FIG. 1. High-resolution energy scans, measured by inelastic neutron scattering, of the transverse acoustic (TA) phonons propagating along [100], and polarized along [010] are plotted. (a) shows the low-$q$ part of the dispersion, where the clearly defined TA mode disperses until 9 meV, as better seen in (b). In (b), we see that the TA mode is cut off by an optical branch at 9 meV. Three higher-energy optical branches are also highlighted using the fit for the $q = 0.45$ r.l.u. point, plotted as a solid black line. Measurements were done on IN8@ILL with a fixed $k_f = 2.662$ Å$^{-1}$.

We have performed an exhaustive investigation of phonon dynamics in YSZ, measuring transversely and longitudinally polarized modes propagating along the main symmetry directions of the cubic structure (see Fig. 2; raw data are reported in the Supplemental Material [26] Appendix F). In Fig. 1, we report some energy scans at constant $Q$ of transverse acoustic phonons propagating along [100], polarized along [010] [$\Delta$(TA) branch], as representative for our major findings. Here, it may be seen that the TA mode disperses and broadens until $q = 0.35$ r.l.u. Above this value, it no longer disperses, remaining pinned to the 9 meV energy position and merging into a continuum of optical modes, with bands centered at 9, 17, 27, and 32 meV.

This is not an isolated case. Figure 2 reports the dispersions in all the probed symmetry directions, as obtained by fitting our data (see Supplemental Material Appendix D [26] and references therein [29]): Here, we observe a similar cutoff of the acoustic branch for the $\Sigma$(TA$_1$) polarization in the [110] direction, while all measured LA polarizations and the $\Sigma$(TA$_2$) polarization along the [110] direction appear to continue dispersing past 9 meV, crossing one or more optical branches along the way before reaching the ends of the respective Brillouin zones. As for the $\Lambda$(TA) polarization in the [111] direction, the acoustic phonon seems to continue past the 9 meV optic mode and merge with the 17 meV optic mode.

As mentioned in the Introduction, optical modes have already been reported by Raman spectroscopy. In a perfect cubic structure, only one Raman-active mode exists, but the presence of defects blurs the polarization of vibrational modes, changing their Raman activity [17]. As a consequence, an optical continuum could be observed, containing several peaked features, from a few meV up to ∼80 meV. Specifically, three main bands could be identified in polarized Raman spectra for an yttria content of $x = 9.5$ mol % as belonging to the $A_{1g}$, $T_g$, and $E_g$ irreducible representations of the crystalline
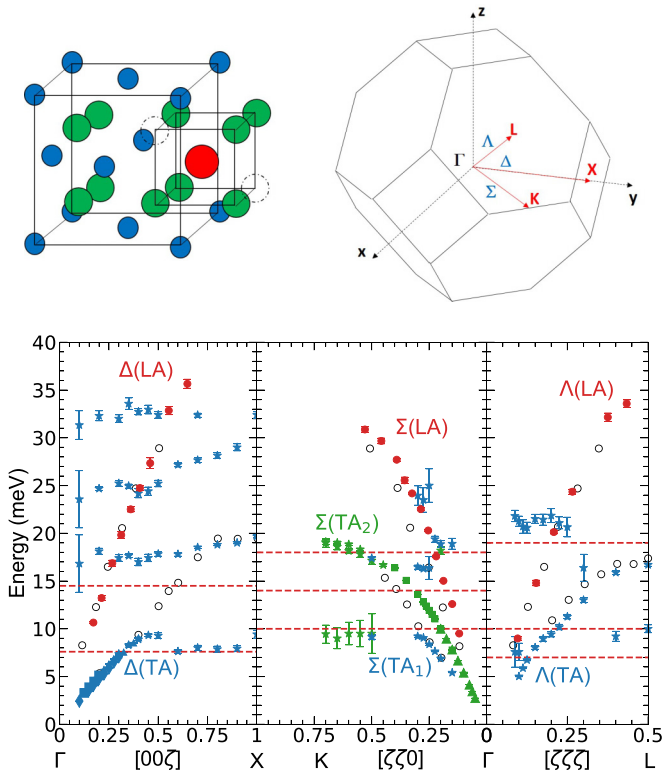
FIG. 2. Top left: Sketch of the cubic YSZ crystalline structure (CaF₂ type, space group No. 225), with Zr atoms in blue, O atoms in green, and Y atoms in red. Open dashed circles indicate O vacancies. Top right: Brillouin zone, with the main symmetry directions reported in red: [100] (Γ-X, Δ direction), the [110] (Γ-K, Σ direction) and the [111] (Γ-L, Λ direction). Bottom: Experimental phonon dispersions at 300 K. The longitudinal acoustic (LA) phonons (red circles) have been measured by IXS, with horizontal lines representing the energies of the optical branches that were fixed in position during analysis. TA phonons (blue) have been measured by INS on 4F2@LLB (diamonds), 1T@LLB with 20′ collimation (triangles), 1T@LLB with 60′ collimation (squares), and IN8@ILL (stars). The second TA polarization in the [ζζ0] direction (green) is similarly a combination of INS setups (same marker symbols apply). Data have been measured around the Bragg peaks (002), (200), (220), (111), and (222) as detailed in Table S1 of the Supplemental Material [26]. Data from Argyriou *et al.* [20] are also reported as open gray circles. The error bars for the leftmost transversely polarized optical branches in the [00ζ] direction represent width rather than error of the energy position.

symmetry group $O_h$ for the cubic fluoride-type structure [23] (see Table S3 of the Supplemental Material [26] and references therein [30]). In all the polarizations, a well-defined peak at 9–10 meV is present. Peaks at 18 and 35 meV appear also in some symmetries, in good agreement with the present measurements.

Our results represent experimental evidence throughout the whole Brillouin zone of optical modes for this material, which, until now, have been elusive within previous investigations. Moreover, we observe a premature end of the acoustic phase space for some transverse branches, where previous studies reported TA modes dispersing up to ∼20 meV. A very
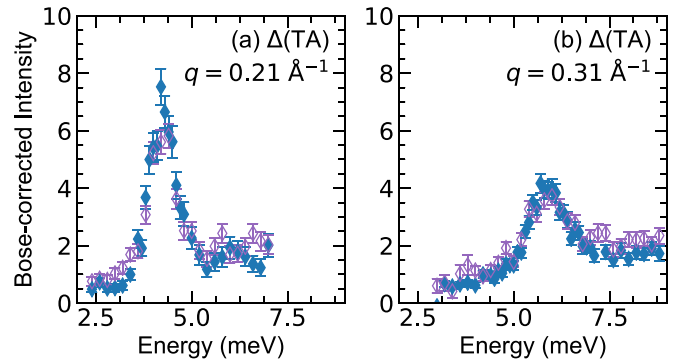


FIG. 3. Temperature dependence of representative energy scans from the transverse acoustic (TA) phonon dispersion in which phonons propagate along [100] and are polarized along [010]. Scans have been made on 4F2@LLB at 300 K (blue) and 50 K (purple) and have been corrected according to the Bose-Einstein distribution.

different scenario therefore arises from our data, which can be understood in terms of an improved experimental resolution. Previous INS experiments have been performed using a fixed $k_f = 4.1$ Å$^{-1}$ [20], in which case the instrumental resolution ellipsoid is large, such that when the acoustic mode approaches the low-lying optical mode, they are no longer clearly resolved, but rather appear as a single mode. The intensity transfer among the different optical bands creates the effect of a dispersive acoustic mode up to 20 meV. And indeed, we have repeated the measurements using the same low instrumental resolution, and found that the optical mode is no longer resolved and the single visible mode disperses similarly to that work (see Supplemental Material Appendix C [26]).

It is worth underlining that a dispersionless mode at 9 meV had already been reported by Cousland *et al.* [19], who measured it along the Σ(LA) branch at three *Q* points. Interestingly, both in their *ab initio* calculations of the density of states and in the ones of Tojo *et al.* [16], a small peak at 8–9 meV is present. Still, the authors did not propose an optical nature for it but rather identified it as a soft longitudinal mode which is normally imaginary in cubic ZrO₂, and would become positive, stabilizing the cubic phase because of phonon-phonon interactions [31].

The temperature dependence of the phonon dynamics has been investigated down to 50 K. In Fig. 3 we report data for the Δ(TA) branch at room and low temperature, after correction by the Bose factor. The good overlap confirms a negligible effect of temperature within our experimental resolution, and thus a negligible role of anharmonicity, pointing instead to a major role of defects, due to oxygen vacancies, in determining phonon attenuation.

The fitted acoustic linewidths are reported in Fig. 4. Unfortunately, we could not extract them for the Σ(TA₁) and the Λ(TA) modes, due to resolution limitations (see Supplemental Material Appendix D [26]).

It is usually expected that a dominant point defect scattering would lead to a Rayleigh-type dependence of the linewidth on the energy, $\Gamma \propto (\hbar\omega)^4$ [32]. Still, extended defect structures could induce a more Mie-type scattering, with a softer dependence, $\Gamma \propto (\hbar\omega)^2$ [33]. Moreover, works on highly
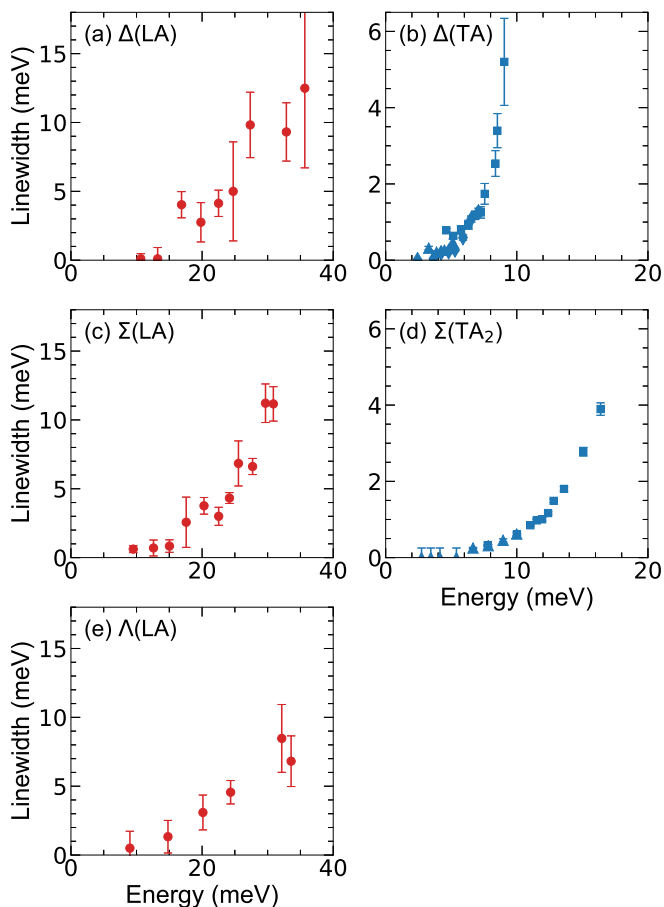
FIG. 4. When possible according to the different experimental setups, intrinsic linewidths have been extracted. Colors and symbols follow from Fig. 2.
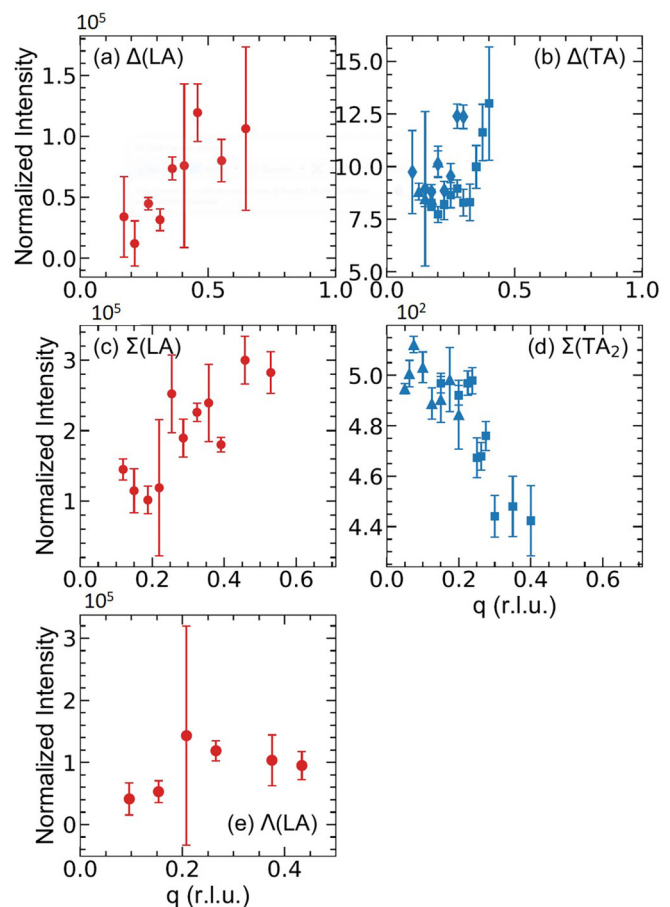


FIG. 5. Normalized intensity at 300 K (colors and symbols as in Fig. 2). Longitudinal acoustic modes have been measured by IXS. All intensities have been normalized by the analyzer efficiency to compare scans across different analyzers. Transverse acoustic modes were measured by various INS setups and have been scaled to match each other in each polarization.

defective crystals such as random alloys [34–38] have reported the presence of several regimes. In YSZ, we find quite clear power laws, with exponents spanning from the Mie-type to the Rayleigh-type scattering: $\Gamma = (\hbar\omega)^x$, with $x = 2.15$, 3.33, and 1.75 for the LA in Figs. 4(a), 4(c), and 4(e), and $x = 5.00$ and 3.89 for TA in Figs. 4(b) and 4(d), respectively.

It is important to notice that the strong increase above 9 meV in the Δ(TA) linewidth is only due to the fact that above this energy we are in fact measuring the width of the optical band. Instead, no change in the broadening regime appears when approaching the low-lying optical mode for phonons which are not stopped in their dispersion. Still, as explained in the Supplemental Material [26] Appendix D, an interaction between optical and acoustic phonons can be unveiled by looking at the normalized acoustic intensity, reported in Fig. 5, which, in the case of a purely acoustic mode, should be constant with $q$ [27,34,39–44]. In the figure, we can see that it departs from a constant value when approaching the optical mode, giving a clear signature of the end of the pure acoustic phonon regime and of an arising interaction with the optic mode.

It is interesting to comment on the different interactions observed between the lowest-lying optical mode and the acoustic branches depending upon their propagation direction and polarization. As seen in Fig. 2, only the Δ(TA) and the Σ(TA₁)

are clearly stopped at 9 meV. A first attempt at understanding this can be made by looking to the nominal polarization direction of the optical mode and its relation to that of the acoustic ones. Using the irreducible representations for a perfect cubic structure, only for these two transverse branches and the LA[100], the scalar product between their nominal polarization and the ones of the two degenerate $E_g$ 9 meV optical modes is nonzero, while this is not the case for all the other acoustic branches, for which the scalar product is zero with at least one of the two degenerate $E_g$ modes. This would indicate that the acoustic dispersion is halted only when both $E_g$ polarizations can interact with the acoustic mode. This however does not apply to the LA[100], despite it having a nonzero scalar product. On the other hand, in a defective structure, polarizations and symmetry are expected to be modified, and they also depend on the $q$ point. As such, in order to definitively shed light on the acoustical-optical interactions in YSZ, a calculation of the polarization and symmetry of both optical and acoustic modes throughout the Brillouin zone is needed. This is even more true since our results clearly indicate that previously calculated phonon dispersions in YSZ are not reliable, as they do not reproduce the early end of the

acoustic phase space in some directions and polarizations, nor the existence of low-lying optical branches.

## III. CONCLUSIONS

In conclusion, we have revisited the lattice dynamics of yttria-stabilized zirconia ($x = 9.5$ mol %) with high-resolution INS and IXS measurements, giving insight into the presence of optical branches throughout the whole Brillouin zone that interact with the acoustic phonon modes and that, in some polarizations, cause the early end of the acoustic branch. Our findings highlight the need for other *ab initio* calculations that consider the true defect structure of YSZ and that allow us to predict the correct phonon dispersions, and, specifically, the presence of defect-induced optical modes and the acoustical-optical interaction.

Finally, these results point to a deeper understanding of thermal transport in YSZ, which was previously interpreted as being due to a huge disorder-induced phonon broadening [20]. It now appears to be the result of two concomitant phenomena at play. Not only is there an important defect-induced scattering, spanning from a Mie to a Rayleigh type, depending on direction and polarization, but there is also a significant reduction in the acoustic phase space. Indeed, for some polarizations and directions, the acoustic transverse mode prematurely ends, at about half the Brillouin zone, and is replaced by a nondispersive optic mode, which, having zero group velocity, does not contribute to propagative heat transport.

To go further and completely understand how the details of the extended defect structure, its length scale, and the anisotropy affect phonon dynamics and thermal transport in YSZ, a similar exhaustive investigation as a function of the yttria content, combined with a deep defect structure study and the support of theoretical calculations, will be needed. This work represents an important step in this direction and will undoubtedly inspire additional theoretical work on this technologically relevant material.

[1] S. M. Meier and D. K. Gupta, The evolution of thermal barrier coatings in gas turbine engine applications, J. Eng. Gas Turbines Power **116**, 250 (1994).

[2] D. R. Clarke and C. G. Levi, Materials design for the next generation thermal barrier coatings, Annu. Rev. Mater. Res. **33**, 383 (2003).

[3] N. P. Padture, M. Gell, and E. H. Jordan, Thermal barrier coatings for gas-turbine engine applications, Science **296**, 280 (2002).

[4] J. D. McCullough and K. N. Trueblood, The crystal structure of baddeleyite (monoclinic ZrO2), Acta Crystallogr. **12**, 507 (1959).

[5] P. Aldebert and J.-P. Traverse, Structure and ionic mobility of zirconia at high temperature, J. Am. Ceram. Soc. **68**, 34 (1985).

[6] D. K. Smith and C. F. Cline, Verification of existence of cubic zirconia at high temperature, J. Am. Ceram. Soc. **45**, 249 (1962).

[7] G. Witz, V. Shklover, W. Steurer, S. Bachegowda, and H.-P. Bossmann, Phase evolution in yttria-stabilized zirconia thermal barrier coatings studied by Rietveld refinement of x-ray powder diffraction patterns, J. Am. Ceram. Soc. **90**, 2935 (2007).

[8] R. Mévrel, J.-C. Laizet, A. Azzopardi, B. Leclercq, M. Poulain, O. Lavigne, and D. Demange, Thermal diffusivity and conductivity of $Zr_{1-x}Y_xO_{2-x/2}$ ($x = 0$, 0.084 and 0.179) single crystals, J. Eur. Ceram. Soc. **24**, 3081 (2004).

[9] M. Fèvre, A. Finel, and R. Caudron, Local order and thermal conductivity in yttria-stabilized zirconia. I. Microstructural investigations using neutron diffuse scattering and atomic-scale simulations, Phys. Rev. B **72**, 104117 (2005).

[10] J.-F. Bisson, D. Fournier, M. Poulain, O. Lavigne, and R. Mévrel, Thermal conductivity of yttria-zirconia single crystals, determined with spatially resolved infrared thermography, J. Am. Ceram. Soc. **83**, 1993 (2004).

[11] M. Fèvre, A. Finel, R. Caudron, and R. Mévrel, Local order and thermal conductivity in yttria-stabilized zirconia. II. Numerical and experimental investigations of thermal conductivity, Phys. Rev. B **72**, 104118 (2005).

[12] T. Welberry, R. Withers, J. Thompson, and B. Butler, Diffuse scattering in yttria-stabilized cubic zirconia, J. Solid State Chem. **100**, 71 (1992).

[13] T. Welberry, B. Butler, J. Thompson, and R. Withers, A 3D model for the diffuse scattering in cubic stabilized zirconias, J. Solid State Chem. **106**, 461 (1993).

[14] T. R. Welberry and B. D. Butler, Interpretation of diffuse x-ray scattering *via* models of disorder, J. Appl. Crystallogr. **27**, 205 (1994).

[15] J. P. Goff, W. Hayes, S. Hull, M. T. Hutchings, and K. N. Clausen, Defect structure of yttria-stabilized zirconia and its influence on the ionic conductivity at elevated temperatures, Phys. Rev. B **59**, 14202 (1999).

[16] T. Tojo, T. Atake, T. Mori, and H. Yamamura, Excess heat capacity in yttria stabilized zirconia, J. Therm. Anal. Calorim. **57**, 447 (1999).

[17] P. K. Schelling and S. R. Phillpot, Mechanism of thermal transport in zirconia and yttria-stabilized zirconia by molecular-dynamics simulation, J. Am. Ceram. Soc. **84**, 2997 (2001).

[18] P. Dalach, D. E. Ellis, and A. van de Walle, First-principles thermodynamic modeling of atomic ordering in yttria-stabilized zirconia, Phys. Rev. B **82**, 144117 (2010).

[19] G. P. Cousland, R. A. Mole, M. M. Elcombe, X. Y. Cui, A. E. Smith, C. M. Stampfl, and A. P. J. Stampfl, Investigation of the vibrational properties of cubic yttria-stabilized zirconia: A

combined experimental and theoretical study, J. Phys. Chem. Solids **75**, 351 (2014).

[20] D. N. Argyriou and M. M. Elcombe, A neutron scattering investigation of cubic stabilised zirconia (CSZ)—II. Lattice dynamics of Y- and Ca-CSZ, J. Phys. Chem. Solids **57**, 343 (1996).

[21] D. W. Liu, C. H. Perry, A. A. Feinberg, and R. Currat, Neutron-scattering studies of phonons in disordered cubic zirconia at elevated temperatures, Phys. Rev. B **36**, 9212 (1987).

[22] D.-J. Kim, H.-J. Jung, and I.-S. Yang, Raman spectroscopy of tetragonal zirconia solid solutions, J. Am. Ceram. Soc. **76**, 2106 (1993).

[23] M. Ishigame and E. Yoshida, Study of the defect-induced Raman spectra in cubic zirconia, Solid State Ionics **23**, 211 (1987).

[24] G. Morell, R. S. Katiyar, D. Torres, S. E. Paje, and J. Llopis, Raman scattering study of thermally reduced stabilized cubic zirconia, J. Appl. Phys. **81**, 2830 (1997).

[25] C. H. Perry, D.-W. Liu, and R. P. Ingel, Phase characterization of partially stabilized zirconia by Raman spectroscopy, J. Am. Ceram. Soc. **68**, C-184 (1985).

[26] See Supplemental Material at http://link.aps.org/supplemental/10.1103/PhysRevMaterials.7.115401 for details of the experimental conditions, data analysis, and sample characterizations.

[27] S. Pailhès, V. M. Giordano, P.-F. Lory, M. D. Boissieu, and H. Euchner, in *Nanostructured Semiconductors*, edited by K. Termentzidis (Pan Stanford, Singapore, 2017).

[28] G. Shirane, S. M. Shapiro, and J. M. Tranquada, *Neutron Scattering with a Triple-Axis Spectrometer* (Cambridge University Press, Cambridge, UK, 2015).

[29] B. Hennion and P. Bourges, AFITV: Refinement program for triple axis spectrometer data at Laboratoire Leon Brillouin, CEA/Saclay, France.

[30] E. Silberman and H. Morgan, Use of group theory in the interpretation of infrared and Raman spectra, Tech. Rep. ORNL/TM–5666, Oak Ridge National Laboratory, 1977 (unpublished).

[31] P. Souvatzis and S. P. Rudin, Dynamical stabilization of cubic $ZrO_2$ by phonon-phonon interactions: *Ab initio* calculations, Phys. Rev. B **78**, 184304 (2008).

[32] J. Callaway, Model for lattice thermal conductivity at low temperatures, Phys. Rev. **113**, 1046 (1959).

[33] R. Guo and S. Lee, Mie scattering of phonons by point defects in IV-VI semiconductors PbTe and GeTe, Mater. Today Phys. **12**, 100177 (2020).

[34] S. R. Turner, S. Pailhès, F. Bourdarot, J. Ollivier, Y. Sidis, J.-P. Castellan, J.-M. Zanotti, Q. Berrod, F. Porcher, A. Bosak, M. Feuerbacher, H. Schober, M. de Boissieu, and V. M. Giordano,

Phonon behavior in a random solid solution: a lattice dynamics study on the high-entropy alloy FeCoCrMnNi, Nat. Commun. **13**, 7509 (2022).

[35] S. Mu, R. J. Olsen, B. Dutta, L. Lindsay, G. D. Samolyuk, T. Berlijn, E. D. Specht, K. Jin, H. Bei, T. Hickel, B. C. Larson, and G. M. Stocks, Unfolding the complexity of phonon quasi-particle physics in disordered materials, npj Comput. Mater. **6**, 4 (2020).

[36] W. A. Kamitakahara and B. N. Brockhouse, Vibrations of a mixed crystal: Neutron scattering from $Ni_{55}Pd_{45}$, Phys. Rev. B **10**, 1200 (1974).

[37] Y. M. Beltukov and D. A. Parshin, Theory of sparse random matrices and vibrational spectra of amorphous solids, Phys. Solid State **53**, 151 (2011).

[38] Y. M. Beltukov and D. A. Parshin, Density of states in random lattices with translational invariance, JETP Lett. **93**, 598 (2011).

[39] M. Boudard, M. de Boissieu, S. Kycia, A. I. Goldman, B. Hennion, R. Bellissen, M. Quilichini, R. Currat, and C. Janot, Optic modes in the AlPdMn icosahedral phase, J. Phys.: Condens. Matter **7**, 7299 (1995).

[40] G. L. Squires, *Introduction to the Theory of Thermal Neutron Scattering* (Cambridge University Press, Cambridge, UK, 2012).

[41] P.-F. Lory, V. M. Giordano, P. Gille, H. Euchner, M. Mihalkovič, E. Pellegrini, M. Gonzalez, L.-P. Regnault, P. Bastie, H. Schober, S. Pailhes, M. R. Johnson, Y. Grin, and M. de Boissieu, Impact of structural complexity and disorder on lattice dynamics and thermal conductivity in the o-$Al_{13}Co_4$ phase, Phys. Rev. B **102**, 024303 (2020).

[42] M. de Boissieu, S. Francoual, M. Mihalkovi, K. Shibata, A. Q. R. Baron, Y. Sidis, T. Ishimasa, D. Wu, T. Lograsso, L.-P. Regnault, F. Gähler, S. Tsutsui, B. Hennion, P. Bastie, T. J. Sato, H. Takakura, R. Currat, and A.-P. Tsai, Lattice dynamics of the Zn-Mg-Sc icosahedral quasicrystal and its Zn-Sc periodic 1/1 approximant, Nat. Mater. **6**, 977 (2007).

[43] P.-F. Lory, Dynamique de réseau et conductivité thermique dans les alliages métalliques complexes, Ph.D. thesis, Université de Grenoble, 2015.

[44] S. Pailhès, H. Euchner, V. Giordano, R. Debord, A. Assy, S. Gomès, A. Bosak, D. Machon, S. Paschen, and M. de Boissieu, Localization of propagative phonons in a perfectly crystalline solid, Phys. Rev. Lett. **113**, 025506 (2014).

[45] S. R. Turner, F. Bourdarot, M. de Boissieu, V. Giordano, A. Ivanov, S. Pailhès, A. Piovano, S. Raymond, and H. Schober, Disentangling anharmonic from disorder dominated thermal transport in yttria stabilized cubic zirconia, doi:10.5291/ILL-DATA.7-01-492 (2019).